International Journal of Semiconductor Science & Technology (IJSST)
ISSN 2250-1576
Vol. 3, Issue 1, Mar 2013, 1-10

EFFECT OF YTTRIUM DOPING ON THE PROPERTIES OF BISMUTH FERRITE: A REVIEW

SUBHABRATA CHAKRABORTY[1], SOUMYA MUKHERJEE[2] & SIDDHARTHA MUKHERJEE[3]

P.G. Scholar, School of Materials Science & Nanotechnology, Jadavpur University, Kolkata-700032, India

PhD Scholar, Department of Metallurgical & Material Engineering, Jadavpur University, Kolkata-700032, India

Professor, Department of Metallurgical & Material Engineering, Jadavpur University, Kolkata-700032, India

ABSTRACT

Multiferroics are those materials which have simultaneous existence of at least two ferroic properties in the same material. Multiferroic magnetolectrics exhibit both ferromagnetic and ferroelectric properties. One of the primary applications of magnetoelectrics is in memory devices, high density data storage etc. An ideal memory material is one that exhibits high saturation magnetization, high remanent magnetization and polarization along with low coercive value. Bismuth ferrite (BFO) is a magnetoelectric material which has drawn quite an attention over the last few years. It has been observed that the multiferroic properties of BFO can be improved significantly by doping with rare earth transition metals. In this paper, we are going to provide a review on the important findings of research investigations on the enhancement of properties of BFO due to yttrium (Y) doping. Hence, the material with enhanced properties can be applied in a number of applications like gas sensors and optical fibers which require essentially high precision.

KEYWORDS: Bismuth Ferrite, Multiferroic, Yttrium Doping, XRD, SEM, FTIR, Raman Spectroscopy

INTRODUCTION

The term “Multiferroic” was coined by Schimd in the year 1994 [1]. Any such material which possesses two or more primary ferroic properties in a single phase can be termed so. However, non-primary ferroic properties such as antiferromagnetism and ferrimagnetism can also be included in the definition. In the early 1960s, the prediction of magnetoelectric coupling was done and later it was seen in chromium(III) oxide, a naturally occurring multiferroic material. In the year 2000, Spaldin elaborated the conditions required for simultaneous existence of ferromagnetism and ferroelectricity in oxides [2]. A paper by Ramesh et al (2003) showed that the BFO films prepared by them had a remanent polarization about 15 times than that in bulk [1]. BFO is a room temperature magnetoelectric having perovskite structure. BFO at room temperature is rhombohedral R3c (Hexagonal system) that exhibits ferroelectricity and antiferromagnetism (G type ordering). The canting of antiferromagnetic sublattice imparts weak ferromagnetism within the system. Due to the presence of spin cycloid ordering, the antiferromagnetic axis rotates with a disproportionate wavelength period of about 62nm cancellin the weak ferromagnetism [3]. It can be applied in memory applications apart from terahertz radiation and spintronics applications. PZT have widely been used in ferroelectric memory applications. BFO is non-toxic and can replace PZT, provided its problems like oxygen and mixed vacancies; high leakage can be mitigated [2].

The material scientists are investigating and concentrated their focus on improving the multiferroic properties of BFO by doping with various elements. Yttrium (Y) is a rare earth transition metal which has

shown good result in this direction of research. When BFO is doped with Y, it occupies the position of bismuth ion. In this article, we are trying to provide on the latest modifications in different aspects of BFO due to Y doping.

EXPERIMENTAL TECHNIQUES

Several researchers have synthesized Y doped BFO (BYFO) in a variety of ways with different precursors. These techniques are broadly classified as follows.

Precursor Solution Evaporation Route

Mishra et al (2008) took stoichometric amounts of nitrate salts of bismuth, iron and yttrium oxide in HNO_3. Trimethylene amine was then added to the solution as complexing agents. The resulting solution was evaporated to form a gel which was then annealed at a temperature between 600ºC, 700ºC, 750ºC for different doping percentages for a desired period of time to get crystalline samples [4].

Bellakki et al (2010) adopted a similar preparation route but used yttrium(II) nitrate as precursor and ion free water as solvent. The complexing agent used here was citric acid. The ratio of number of moles of citric acid to the total number of moles of nitrate salts was maintained at 1:1 [5].

Hydrothermal Method

Stoichometric amounts of nitrate salts were taken and pH of the solution was adjusted using KOH as mineralizer. Then the solution was centrifuged to get a reddish-brown precipitate, which was dispersed ultrasonically and then transferred to a Teflon-lined stainless steel autoclave. The autoclave was then placed in an oven at 220ºC for 6hrs. After hydrothermal treatment, the autoclave was cooled to room temperature and the final products were filtered and washed in 10% nitric acid and distilled water to remove all soluble salts and then dried at 90ºC in an oven for 1hr [6].

Modified Pechini Route

Stoichometric amounts of nitrate salts of bismuth and yttrium in distilled water were mixed with equal moles of iron nitrate in distilled water and ultrasonicated for 2hrs. Nitric acid was used to adjust the pH of the solution to 2. Then the solution was added to maleic acid solution under ultrasonication. Polyethelyne glycol was then added and the solution was ultrasonicated for 3hrs. The molar ratio of polyethylene glycol to maleic acid should be 1:1. The resulting solution was evaporated and annealed at 600ºC for 2hrs [7].

Sol-Gel Route

Gautam et al (2012) took stoichometric amounts of nitrate salts of bismuth, iron and yttrium(II) along with citric acid. Ethylene glycol was then added as a complexing agent. The resulting solution was then evaporated to form a xerogel and annealed at 600ºC to obtain the samples [8].

Chen et al (2012) adopted a similar route with a slight variation in the process parameters. The solvent used was nitric acid and the complexing agent was tartaric acid.In order to remove hydrocarbon and NO_x impurities, the samples were preheated before annealing [9].

Luo et al (2012) took tartaric acid as complexing agent along with the nitrate salts in distilled water. They dried the solution at 150ºC followed by annealing at 600ºC for 2hrs. The obtained powder was dried,

pressed into discs and sintered at 700ºC for 30mins. They also used 4% excess bismuth to compensate for its loss during heat treatment [10].

Solid State Route

Oxides of bismuth, iron and yttrium are weighed and ball milled. After drying the mixture, it is calcined at about 780ºC for 2hrs. Then the powder is again ball milled, granulated using binding agents like polyvinyl alcohol and pressed into discs and again sintered at temperature 850ºC for pure samples and at 870ºC for doped samples [11].

PHASE ANALYSIS BY XRD AND EDX

The research works carried on rare earth metal doping of BFO have confirmed a change in c/a ratio or in other words, a structural change occurs. According to Mishra et al (2008), doping of yttrium in BFO within the percentage range ($\leq$ 10%), results in rhombohedral system but beyond this, it is tetragonal. The calculated values of lattice strain was found to be increasing due to yttrium doping upto 10%, while it decreases slightly at 15% [4]. Bellakki et al (2010) reported that beyond 10%, there was a significant amount of impurity formation and a structural change. Thus, 10% of Y doping in BFO can be regarded as its solid-solubility limit [5]. Hou et al (2011) has reported that for 5% Y doping crystal structure of BFO does not change, however a lattice strain is induced due to Y^{3+} substitution [6]. Mukherjee et al (2012) have reported the formation of second phase $Bi_2Fe_4O_9$ for $\leq$10% doping and above it the secondary phase disappears [7]. Gautam et al (2012) have reported that the impurities vanish on yttrium substitution and lattice paremeters decrease. This is because of the fact that they used $Y(NO_3)_2$ as the precursor and Y^{2+} is smaller than Bi^{3+} ion. The stability of perovskite compound was determined by calculating the tolerance factor (t), given as:

$$t = r_A + r_O / \sqrt{2}\ (r_B + r_O) \quad (1)$$

Where, r_A was the average ionic radii of Bi^{3+} and Y^{3+} ions, r_B was the average ionic radii of Fe^{3+} and Fe^{4+} ions, r_O was the ionic radius of O^{2-} ion. They have reported a continuous decrease in value of t indicating a structural transition [8].

Chen et al (2012) have observed a reflection (111) plane for 10% Y doping along with an orthorhombic structured sample. However, below this doping percentage, the structure was found to be rhombohedral [9].

Lou et al (2012) found a structural transition to orthorhombic with $Pn2_{1a}$ space group with a doping of $\geq$10% [10].

Feng et al (2010) found a secondary phase of $Bi_2Fe_4O_9$ in their sample which vanished on Y^{3+} substitution. However, they found the presence of $Y_3Fe_5O_{12}$ in the doped samples [11].

EDX analyses have confirmed that lanthanum ions, when doped in BFO, occupy the lattice positions [13, 17]. The EDX analyses of the samples of Bellakki et al (2010) have showed the presence of bismuth and yttrium in appropriate ratio [5].

MORPHOLOGICAL ANALYSES

The precursor solution evaporation method gave agglomerated particles along with high interconnection of grains with a particle size ranging between less than 1µm [5].

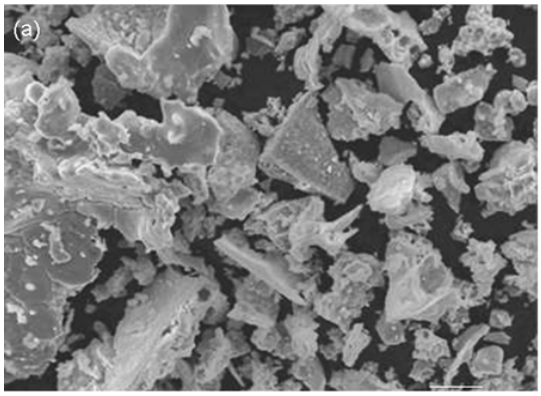

Figure 1: SEM Micrograph of BFO Samples; Magnification-1000; Scale Bar-10µm [5]

The sol-gel technique adopted by Gautam et al (2012) gave agglomerated clusters of spherical particles [8]. Feng et al (2010) found that solid state route gives polyhedral particles and the size of the formed samples decrease upon doping. Further, as the doping concentration was increased the particle size decreased [11].

FTIR ANALYSES

Mishra et al (2008) found a strong absorption peak near 547cm^{-1} and 435cm^{-1} which were due Fe-O stretching and bending vibrations respectively [4]. This result was in agreement with the study of lanthanum doped BFO by Chen et al (2011), where they also found low intensity peaks due to O-H stretching in the calcined gel and hydrothermally treated 3% lanthanum doped BFO samples [12]. Mukherjee et al (2012) upon FTIR studies of the doped samples found similar results. Along with the aforesaid peaks, they also found peak due to O-H bending at 1700cm^{-1} and a peak at 1390cm^{-1} due to trapped nitrates. The band at 1300cm^{-1} were due to formation of esters because of condensation during gelation and peaks due to carbonate groups were found within 1500cm^{-1} to 1300cm^{-1}, 1120cm^{-1} to 1070cm^{-1} and 850cm^{-1} [7].

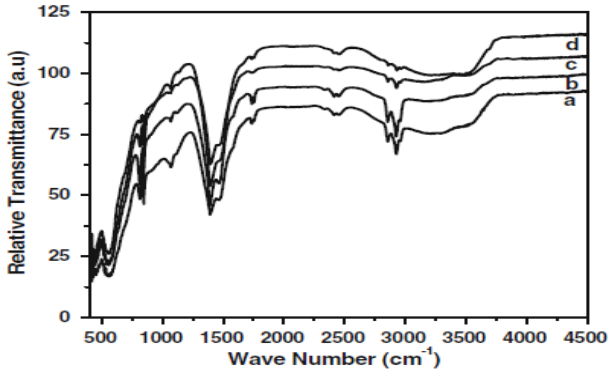

Figure 2: FTIR Spectra of 1%, 5% and 10% Y Doped BFO Samples [7]

XPS ANALYSES

XPS is done to measure the electronic state of an element in a sample. The Fe 2p core level is split into Fe $2p_{1/2}$ and Fe $2p_{3/2}$. For Fe^{3+} and Fe^{2+} ions, Fe $2p_{3/2}$ core level comes at 710.8eV and 709.4eV respectively [14]. Bellakki et al (2010), upon doing XPS characterization of their sample found a main peak at 710.9eV along with two satellite peaks at 718.9eV and 724.4eV. The difference of 8eV between the first two

peaks gives the presence of Fe^{3+} ions in the sample [5]. This is consistent with the report of Zhang et al (2006) on lanthanum doped BFO ceramics [15].

DT-TG ANALYSES

It is known that Curie temperature of BFO is 1100K and its Néel temperature is 643K. Bellakki et al (2010) found that as the doping percentage increased the non-stoichometric oxygen content of the samples decreased [5]. Gautam et al (2012) found that upon Y doping on BFO the Curie temperature increases while Néel temperature decreases. This was in agreement of the fact that perovskites with low tolerance factor have high Curie temperature [8]. Chen et al (2012) found that on Y doping and progressively increasing doping percentage leads to decrease in both Curie and Néel temperatures. The decrease in Curie temperature was attributed to decrease in cell volume due to Y substitution [9]. This observation was in agreement to the observation of Yan et al (2010) [13]. The increase in the curie temperature as reported by Gautam et al (2012) was due to the fact that they used yttrium(II) nitrate as precursor and Y^{2+} is smaller than Bi^{3+} which led to decreased cell parameters hence low tolerance factor and high curie temperature [8].

RAMAN SPECTRA ANALYSES

The Raman active mode of rhombohedral BFO with R3c space group is $4A_1 + 9E$ and that for orthorhombic BFO with Pnma space group is $7A_g + 5B_{1g} + 7B_{2g} + 5B_{3g}$ [3,9]. Chen et al (2012) found 4 strong peaks and 8 weak peaks relative to A_1(TO) and E(TO) modes respectively. The intensity of A_1(TO) peaks at $143cm^{-1}$ and $175cm^{-1}$ decreased while that of E(TO) peak at $124cm^{-1}$ increased with Y substitution due to change in Bi-O bond. They also observed that by increasing doping percentage towards 10%, the stereo chemical activity of electron lone pair of bismuth gets reduced [9]. Lou et al (2012) observed 3 A_1(LO) phonon peaks at $140cm^{-1}$, $172cm^{-1}$ and $218cm^{-1}$and 2 E(TO) phonon peaks at $261cm^{-1}$ and $274cm^{-1}$ in BFO. At 10% Y doping, the intensity of peaks decrease and A_1(LO) peaks shift to higher frequency. However, at 20% doping the peaks disappeared and three new peaks at $310cm^{-1}$, $522cm^{-1}$ and $618cm^{-1}$ became prominent [10]. Feng et al (2010) found 4 A_1 and 6 E modes, although they observed a peculiarity that the Raman active mode of rhombohedral R3c was not $4A_1 + 9E$. They also found a mode at $475cm^{-1}$ in the doped samples [11].

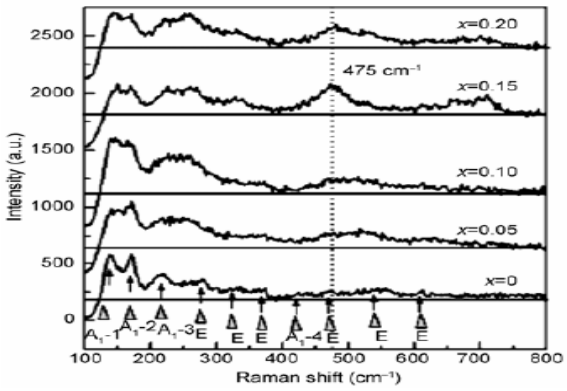

Figure 3: RAMAN Spectra for Various Doping Percentages of Y Doped BFO [11]

TEM-SAED ANALYSES

TEM-SAED analyses can prove to be instrumental in determining the interplanar distance and shape of the formed samples along with the effects of substitution of dopant on the morphology of samples [13, 15, 16].

Mukherjee et al (2012) upon doing TEM-SAED and particle size distribution analyses of their sample have found the average particle size about 29nm with standard deviation of 1.6nm. The lattice spacings were 3.9Å and 2.9Å relative to (101) and (012) planes respectively for rhombohedral BFO [7].

UV-VIS AND PHOTOLUMINESCENCE ANALYSES

The optical bandgap of BFO at room temperature is about 2.8eV and with the increase in temperature it decreases and becomes zero at γ-phase. Thus, BFO shows a metal to insulator transition [1]. Bellakki et al (2010) carried out UV-Vis analysis of their samples and observed that with increase in doping percentage of Y, optical absorption edge energy of BFO gets reduced, thus signaling enhanced photocatalytic activity [5]. Mukherjee et al (2012), however, found that as the doping percentage was increased there was a blue shift of 100nm in the UV-Vis absorption peak and thus, an increase in optical bandgap. The PL spectra of all the samples showed broad emission bands within 550nm to 700nm and no shift in position of the peaks due to doping [7].

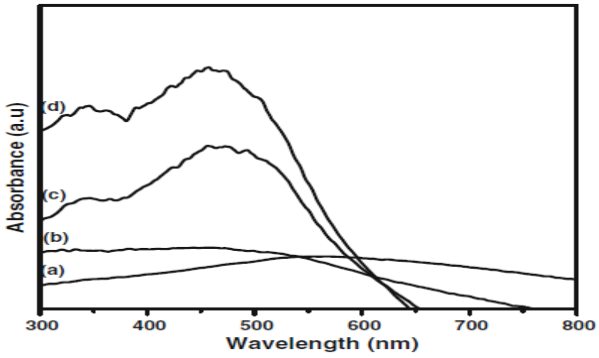

Figure 4: UV-Vis Spectra of (a) Pure BFO, (b) 1% Y Doped BFO, (c) 5% Y Doped BFO, (d) 10% Y Doped BFO [7]

FERROELECTRIC PROPERTIES

Polarization (P) vs. electric field (E) plot at 20 Hz of the samples prepared by Mishra et al (2008) showed low remanent polarization (Pr) and 15% Y doped sample showed a very lossy character [4]. Lou et al (2012) observed improved ferroelectric behaviour of their samples with increase in Y doping percentage due to decreased oxygen vacancies and hence decreased leakage current [10]. Feng et al (2010) have reported that their samples showed a reduction in leakage and widening of hysteresis loops as the doping percentage of Y is increased. However, at a doping of 20%, the ferroelectricity is hardly observed due to YIG phase and smaller grain size [11].

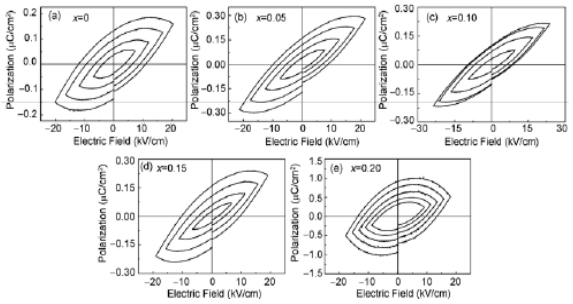

Figure 5: P-E Loops of BFO for Various Doping Percentages of Y [11]

The observations above are consistent with the reports of lanthanum doped BFO, where the P_r value has increased on doping but has decreased slightly at 20% doping and the coercive field values have decreased with doping. The enhancement of ferroelectric properties can be due to the distortion in the structure induced by doping [14, 15, 17, 18 - 21].

DIELECTRIC PROPERTIES

Permittivity (ε_r) and loss tangent (tanδ) measurements of BFO by Mishra et al (2008) done at 35ºC showed dispersive characteristics due to presence of oxygen vacancies but on doping with Y upto 10% it was controlled. On 15% Y doping the dispersions reemerged due to increase in mobile charges and space charge polarization. In case of ε_r and tanδ studies against temperature at 100kHz, an anomaly was found in case of ε_r at 192ºC of BFO due to oxygen vacancy and Fe^{3+}/Fe^{2+} redox interaction. However, on doping this interaction got stabilized and the anomaly disappeared. On 15% Y doping the value of both ε_r and tanδ was found higher than any other lower doping percentages due to ferroelectric to paraelectric transition or magnetoelectric coupling or both [4]. Hou et al (2011) have reported that due to 5% Y doping, the real and imaginary part of permittivity both decrease, however they found the opposite in case of permeability. The loss tangent also decreased with the shifting of relaxation peak to a lower frequency [6]. Gautam et al (2012) found that frequency response of dielectric constant and loss tangent of Y doped BFO decreased a little upto 10kHz and became constant at 1MHz.The trend was that at low frequency both of these were higher as the space charges could follow the field. But in higher frequencies, the space charges could not follow the field and hence the decrease in the respective values. The temperature variations showed anomalies near Néel temperature of BFO [8]. Feng et al (2010) found that on doping both dielectric constant and loss tangent increase at lower frequencies but at higher frequencies the respective values decrease due to space charge relaxation. The temperature measurements showed the dielectric constant values to be increasing initially with temperature followed by a drop at certain point. The anomalies near Néel temperature were observed as expected [11].

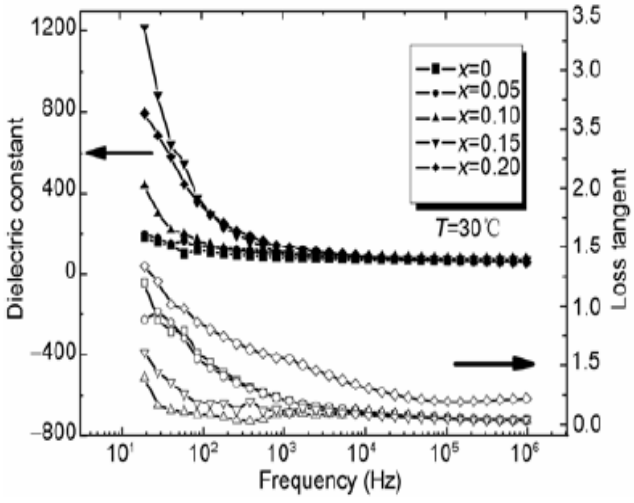

Figure 6: Frequency Dependence of ε_r and tanδ of BYFO Samples [11]

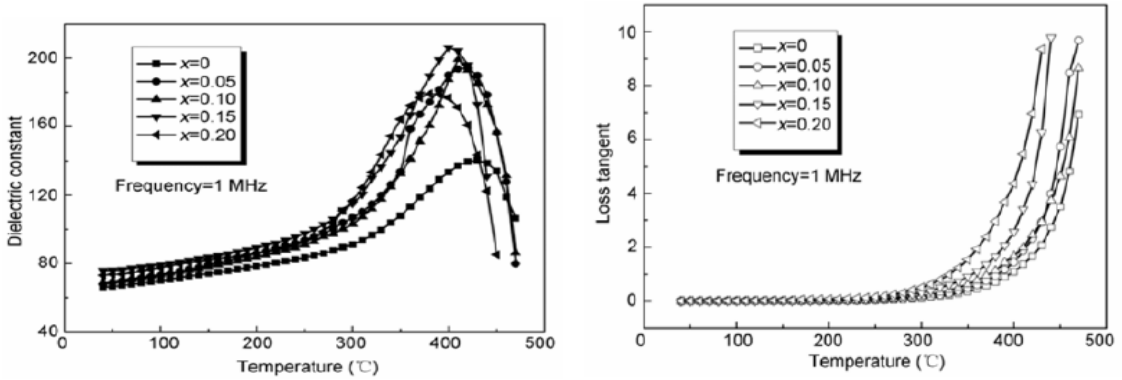

Figure 7: Temperature Dependence of ε_r and tanδ of BYFO Samples [11]

The aforesaid observations are consistent with the studies on lanthanum doped BFO samples [14, 16, 18 - 22].

MAGNETIC PROPERTIES

Due to the spin cycloid structure superimposed upon the antiferromagnetic sublattice, the weak ferromagnetism of BFO at room temperature vanishes. Hence, in order to increase the magnetization, Mishra et al (2008) on doping BFO with yttrium found out that the magnetization of BFO gets enhanced. They also reported that a steep rise in magnetization of BFO was found at low temperatures. They found that at 2K the hysteresis loops of all the samples showed a deviation from room temperature and thus imparting a switchable behaviour to the samples [4]. Bellakki et al (2010) observed that magnetic succeptibility increased with yttrium doping until it reaches 10% at which it drops. This could be due to the structural transition of BFO from rhombohedral to orthorhombic as it changes the coordination number of iron from 6 to 4 and thus the magnetic coupling decreases [5]. Hou et al (2011) found a similar result and they attributed this to the change of Fe-O-Fe bond angle due to doping or in other words to the structural change of the doped samples [6]. Gautam et al (2012), Chen et al (2012) and Feng et al (2010) reported similar results of increased magnetization with yttrium doping. They also reported that below 10% doping, the increase in mgnetization is only due to the suppression of the spin cycloid but above 10% the structural change destroys the spin cycloid completely thus giving a significant increase in magnetization [8, 9, 11].

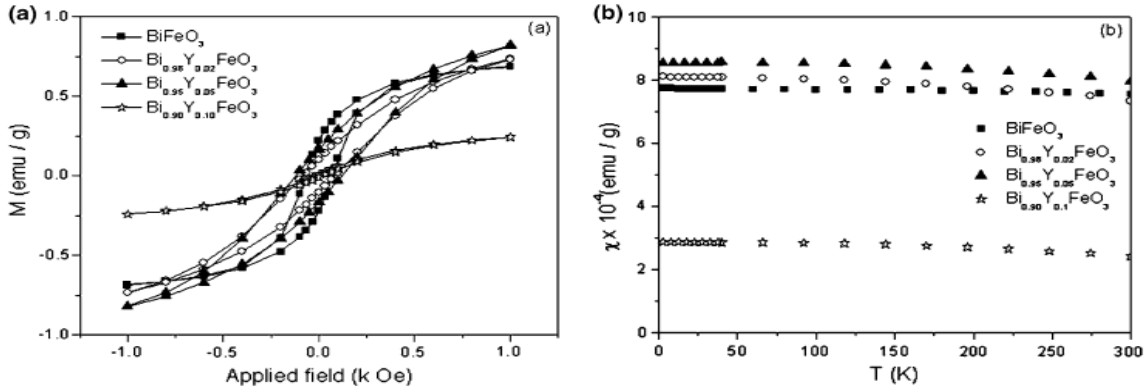

Figure 8: (a) M-H Curve of BFO Samples; (b) Succeptibility Variation with Temperature of BFO Samples [5]

However, Lou et al (2012) observed a clear hysteresis only above 30% Y doping and attributed it to the suppression of spin cycloid and canting of antiferromagnetic sublattice [10].

CONCLUSIONS

From this study we can conclude, to make BFO implementable in device fabrication, yttrium doping is a very effective strategy. The lattice distortion caused by doping is one of the principal causes behind the enhancement in multiferroic properties. If the size is reduced below 62nm then spin cycloid is destroyed thus releasing the suppressed magnetization. Again, the structural distortion causes increase in canting angle and variation of Fe^{2+} ion can also lead to increased magnetization. Finally we can conclude that the, yttrium doped BFO possesses enhanced photocatalytic activity along with multiferroic properties which makes it suitable for device applications. In future, studies of the leakage properties and conductivity of the yttrium doped BFO samples can be done. It has been seen that doping with other rare earth ions like lanthanum, the leakage current also get reduced. For optical fiber applications, the absorption capacity of the material need to be checked and sensitivity of the material should also be enhanced for multiferroic sensor applications.

REFERENCES

1. Catalan, G., & Scott, J. F. (2009). Physics and Applications of Bismuth Ferrite. Advanced Materials, 21, 2463-2485
2. Eerenstein, W., Mathur, N. D., & Scott, J. F. (2006). Multiferroic and magnetoelectric materials. Nature, 442, 759-765
3. Yao, Y., Liu, W., Chan, Y., Leung, C., Mak., C., & Ploss, B. (2011). Studies of Rare-Earth-Doped $BiFeO_3$ Ceramics. International Journal of Applied Ceramic Technology, 8 [5], 1246-1253
4. Mishra, R. K., Pradhan, D. K., Choudhary, R. N. P., & Banerjee, A. (2008). Effect of yttrium on improvement of dielectric properties and magnetic switching behavior in $BiFeO_3$. Journal of Physics: Condensed Matter, 20, 045218, 1-6
5. Bellakki, M. B., & Manivannan, V. (2010). Citrate-gel synthesis and characterization of yttrium-doped multiferroic $BiFeO_3$. Journal of Sol-Gel Science and Technology, 53, 184-192
6. Hou, Z. L., Zhou, H. F., Yuan, J., Kang, Y. Q., Yang, H. J., Jin, H. B., & Cao, M. S. (2011). Enhanced Ferromagnetism and Microwave Dielectric Properties of $Bi_{0.95}Y_{0.05}FeO_3$ Nanocrystals. Chinese Physics Letters, 28 [3], 037702-1-037702-4
7. Mukherjee, A., Hossain, S. M., Pal, M., & Basu, S. (2012). Effect of Y-doping on optical properties of multiferroics $BiFeO_3$ nanoparticles. Applied Nanoscience. DOI 10.1007/s13204-012-0114-8
8. Gautam, A., Uniyal, P., Yadav, K. L., & Rangra, V. S. (2012). Dielectric and magnetic properties of $Bi_{1-x}Y_xFeO_3$ ceramics. Journal of Physics and Chemistry of Solids, 73, 188-192
9. Chen, X. K., Wu, Y. J., Zhang, J., & Chen, X. J. (2012). Giant magnetic enhancement across a ferroelectric-antiferroelectric phase boundary in $Bi_{1-x}Y_xFeO_3$. Science China Physics, Mechanics & Astronomy, 55 [3], 404-408

10. Lou, L., Wei, W., Yuan, X., Shen, K., Xu, M., & Xu, Q. (2012). Multiferroic properties of Y-doped $BiFeO_3$. Journal of Alloys and Compounds, 540, 36-38

11. Feng, B. L., Xue, H., & Xiong, Z. X. (2010). Structure and multiferroic properties of Y-doped $BiFeO_3$ ceramics. Chinese Science Bulletin, 55 [4-5], 452-456

12. Chen, Z., Hu, J., Lu, Z., & He, X. (2011). Low-temperature preparation of lanthanum-doped $BiFeO_3$ crystallites by a sol-gel-hydrothermal method. Ceramics International, 37, 2359-2364

13. Yan, X., Chen, J., Qi, Y., Cheng, J., & Meng, Z. (2010). Hydrothermal synthesis and characterization of multiferroic $Bi_{1-x}La_xFeO_3$ crystallites. Journal of European Ceramic Society, 30, 265-269

14. Gao, F., Cai, C., Wang, Y., Dong, S., Qiu, X. Y., Yuan, G. L., Liu, Z. G, & Liu, J. M. (2006). Preparation of La-doped $BiFeO_3$ thin films with Fe^{2+} ions on Si substrates. Journal of Applied Physics, 99, 094105-1-094105-4

15. Zhang, S. T., Pang, L. H., Zhang, Y., Lu, M. H., & Chen, Y. F. (2006). Preparation, structures, and multiferroic properties of single phase $Bi_{1-x}La_xFeO_3$ (x = 0-0.40) ceramics. Journal of Applied Physics, 100, 114108-1-114108-6

16. Chaudhuri, A., & Mandal, K. (2012). Enhancement of ferromagnetic and dielectric properties of lanthanum doped bismuth ferrite nanostructures. Materials Research Bulletin, 47, 1057-1061

17. Chen, Z., Li, Y., Wu, Y., & Hu, J. (2012). Hydrothermal synthesis and mechanism and property study of La-doped $BiFeO_3$ crystallites. Journal of Materials Science: Materials in Electronics, 23, 1402–1408

18. Lee, Y. H., Wu, J. M., & Lai, C. H. (2006). Influence of La doping in multiferroic properties of $BiFeO_3$ thin films. Applied Physics Letters, 88, 042903-1-042903-3

19. Singh, S. K., Maruyama, K., & Ishiwara, H. (2007). The influence of La-substitution on the micro-structure and ferroelectric properties of chemical-solution-deposited $BiFeO_3$ thin films. Journal of Physics D: Applied Physics, 40, 2705-2709

20. Das, S. R., Bhattacharya, P., Choudhary, R. N. P., & Katiyar, R. S. (2006). Effect of La substitution on structural and electrical properties of $BiFeO_3$ thin film. Journal of Applied Physics, 99, 066107-1-066107-3

21. Yan, F., Zhu, T. J., Lai, M. O., & Lu, L. (2010). Enhanced multiferroic properties and domain structure of La-doped $BiFeO_3$ thin films. Scripta Materialia, 63, 780-783

22. Pandit, P., Satapathy, S., & Gupta, P. K. (2011). Effect of La substitution on conductivity and dielectric properties of $Bi_{1-x}La_xFeO_3$ ceramics: An impedance spectroscopy analysis. Physica B, 406, 2669-2677